Reddening, Emission-Line, and Intrinsic Absorption Properties in the Narrow-Line Seyfert 1 Galaxy Akn 564[1]

D.M. Crenshaw[2,3], S.B. Kraemer[4], T.J. Turner[5,6], S. Collier[7], B.M. Peterson[7], W.N. Brandt[8], J. Clavel[9], I.M. George[5,6], K. Horne[10,11], G.A. Kriss[12], S. Mathur[7], H. Netzer[13], R.W. Pogge[7], K.A. Pounds[14], P. Romano[7], O. Shemmer[13], and W. Wamsteker[9],

ABSTRACT

[1]Based on observations made with the NASA/ESA Hubble Space Telescope. STScI is operated by the Association of Universities for Research in Astronomy, Inc. under NASA contract NAS5-26555.

[2]Department of Physics and Astronomy, Georgia State University, Astronomy Offices, One Park Place South SE, Suite 700, Atlanta, GA 30303

[3]crenshaw@chara.gsu.edu

[4]Catholic University of America and Laboratory for Astronomy and Solar Physics, NASA's Goddard Space Flight Center, Code 681, Greenbelt, MD 20771

[5]Laboratory for High Energy Astrophysics, Code 660, NASA's Goddard Space Flight Center, Greenbelt, MD 20771

[6]Joint Center for Astrophysics, Physics Department, University of Maryland, Baltimore County, 1000 Hilltop Circle, Baltimore, MD 21250

[7]Department of Astronomy, The Ohio State University, 140 West 18th Avenue, Columbus, OH 43210

[8]Department of Astronomy & Astrophysics, The Pennsylvania State University, 525 Davey Laboratory, University Park, PA 16802

[9]ESA, P.O. Box 50727, 28080 Madrid, Spain

[10]School of Physics and Astronomy, University of St. Andrews, St. Andrews, KY16 9SS, UK

[11]Department of Astronomy, University of Texas, Austin, TX 78704

[12]Space Telescope Science Institute, 3700 San Martin Drive, Baltimore, MD 21218

[13]School of Physics and Astronomy and the Wise Observatory, The Raymond and Beverly Sackler Faculty of Exact Sciences, Tel Aviv University, Tel Aviv 69978, Israel

[14]Department of Physics and Astronomy, University of Leicester, University Road, Leicester, LE1 7RH, UK

We use *Hubble Space Telescope* UV and optical spectra of the narrow-line Seyfert 1 (NLS1) galaxy Akn 564 to investigate its internal reddening and properties of its emission-line and intrinsic UV absorption gas. We find that the extinction curve of Akn 564, derived from a comparison of its UV/optical continuum to that of an unreddened NLS1, lacks a 2200 Å bump and turns up towards the UV at a longer wavelength (4000 Å) than the standard Galactic, LMC, and SMC curves. However, it does not show the extremely steep rise to 1200 Å that characterizes the extinction curve of the Seyfert 1 galaxy NGC 3227. The emission-lines and continuum experience the same amount of reddening, indicating the presence of a dust screen that is external to the narrow-line region (NLR). Echelle spectra from the Space Telescope Imaging Spectrograph show intrinsic UV absorption lines due to Lyα, N V, C IV, Si IV, and Si III, centered at a radial velocity of -190 km s^{-1} (relative to the host galaxy). Photoionization models of the UV absorber indicate that it has a sufficient column (N_H = 1.6 x 10^{21} cm^{-2}) and is at a sufficient distance from the nucleus (D > 95 pc) to be the source of the dust screen. Thus, Akn 564 contains a dusty "lukewarm absorber" similar to that seen in NGC 3227.

Subject headings: galaxies: individual (Akn 564) – galaxies: Seyfert

1. Introduction

Narrow-line Seyfert 1 (NLS1) galaxies were first introduced as a class of active galactic nuclei (AGN) by Osterbrock and Pogge (1985). Their optical spectra show narrow (FWHM < 2000 km s^{-1}) permitted and forbidden lines, similar to Seyfert 2 galaxies, but their emission-line ratios are more like those of Seyfert 1 galaxies. In particular, Osterbrock and Pogge found that while the permitted lines are only slightly broader than the forbidden lines, these objects show strong Fe II emission and [O III] λ5007/Hβ ratios < 3, indicating the presence of high density gas like that in the broad-line region (BLR) of Seyfert 1 galaxies. These authors note that the Hβ equivalent widths of NLS1s are smaller than typical values for normal Seyfert 1s, suggesting that they are not just normal Seyfert 1s seen at a special viewing angle.

Renewed interest in NLS1s occurred when it was discovered that they have distinctive X-ray properties; they show a steep soft X-ray excess with a photon index $\Gamma > 3$ below 1 – 2 keV, a steep hard X-ray continuum with Γ = 1.9 to 2.6, and rapid large-amplitude X-ray variability on timescales of minutes to hours (Leighly 1999, and references therein). In addition, optical studies have established that NLS1s lie at one end of the Boroson &

Green (1992) eigenvector 1 for low-redshift quasars and Seyfert 1 galaxies in that they show relatively strong Fe II emission and weak [O III] emission (Boller, Brandt, & Fink 1996).

Akn 564 (z = 0.02467 and D = 99 Mpc, assuming $H_0 = 75$ km s^{-1} Mpc^{-1}) is one of the brightest NLS1s in the X-ray band (Boller et al. 1996), and shows intrinsic UV absorption lines in *HST* spectra (Crenshaw et al. 1999). In order to explore the varability characteristics of a NLS1 in different wave bands, we recently conducted a multiwavelength campaign on Akn 564. The optical monitoring campaign covered the periods 1998 November – 1999 November and 2000 May – 2001 January, and is described by Shemmer et al. (2001). The UV campaign with the *Hubble Space Telescope* was carried out on 2000 May 9 – 2000 July 8 and is described by Collier et al. (2001). Concurrent *RXTE* and *ASCA* observations are described in Pounds et al. (2001) and Turner et al. (2001a), respectively. In this paper, we use the *HST* observations to explore the internal reddening in Akn 564 and the physical conditions in the absorbing gas.

2. Observations

HST spectra of the nucleus of Akn 564 include those obtained with the Faint Object Spectrograph (FOS) and the Space Telescope Imaging Spectrograph (STIS). The details of these observations are summarized in Table 1. We retrieved the flux-calibrated FOS spectra of Akn 564, as well as those of the NLS1 galaxy Mrk 493 for comparison, from the *HST* archives (see Crenshaw et al. [1999] for details on the Mrk 493 observations). We combined these spectra in their regions of overlap to produce UV/optical spectra for both Seyferts in the region 1150 – 6800 Å. The FOS UV spectra are discussed in Crenshaw et al. (1999); Akn 564 shows strong intrinsic absorption lines in Lα, N V $\lambda\lambda$1238.8, 1242.8, Si IV $\lambda\lambda$1393.8, 1402.8, and C IV $\lambda\lambda$1548.2, 1550.8, whereas Mrk 493 shows no evidence for intrinsic absorption. The large wavelength coverage of these spectra is particularly useful for determining the reddening curve of Akn 564 (§3) and the measured fluxes of a large number of UV/optical emission lines (§4) through a fixed aperture (0″.86 in diameter).

As previously mentioned, the STIS spectra were obtained in an intensive monitoring campaign in 2000 May – July. Collier et al. (2001) give the details of the monitoring sequence and data reduction. For the current study, we used the low-dispersion G140L and G230L spectra averaged over 46 visits to assist in the identification of emission features and continuum regions in the UV. We note that the UV continuum fluxes varied mildly during this period (the ratio of maximum to minimum flux at 1360 Å was 1.29) and that the FOS UV continuum fluxes lie within this range; they are lower than those of the average STIS values by a factor of only 0.89 $\pm$0.02. The FOS and STIS emission-line fluxes are also the

same to within 10%.

As part of the STIS campaign, we observed the nucleus of Akn 564 at high spectral resolution (7 km s^{-1} FWHM) with the E140M grating (see Table 1). Our reduction of the E140M spectra included a procedure to remove the background light from each order using a scattered light model devised by Lindler (1998). The individual orders in each echelle spectrum were spliced together in the regions of overlap, and the four individual echelle spectra were weighted by exposure time and averaged to produce a final E140M spectrum. This spectrum was used in Collier et al. (2001) to evaluate the contamination of the emission lines by the absorption lines. In this paper, we use the echelle observations to study the nature of the intrinsic UV absorption in this object (§5).

3. The Reddening Curve in Akn 564

In Figure 1, we show the FOS UV/optical spectra of Akn 564 and Mrk 493 (the latter has been scaled and offset as described in the caption). The smooth curves are spline fits to continuum regions that are free of obvious contamination by absorption or emission lines, including the "little blue bump" between 2200 and 4200 Å, which consists of a blend of broad Fe II and Balmer recombination emission (Wills, Netzer, & Wills 1985). The continuum spectrum of Akn 564 is clearly much flatter than that of Mrk 493 in the UV. This suggests that the spectrum of Akn 564 may experience a significant amount of internal reddening. This is supported by the findings of Walter & Fink (1993), who conclude that Akn 564 is internally reddened based on the large observed Hα/Hβ ratio (= 4.4) and the small ratio of ultraviolet to X-ray continuum flux compared to most Seyfert 1 galaxies (normal and NLS1s) in their sample. These measurements indicate significant internal reddening of the emission lines and UV/optical continuum, since reddening due to our Galaxy is small (see below). We present additional evidence for internal reddening, based on the He II λ1640/λ4686 ratio, in §4.3.

To determine the reddening curve for Akn 564, we used the FOS spectrum of Mrk 493 as a template. We assume that the UV/optical continuum of Mrk 493 is 1) unreddened, except for a small Galactic reddening of E(B−V) = 0.03 (Schlegel et al. 1998), and 2) represents the intrinsic continuum of Akn 564. The first assumption is based on the large rise of the Mrk 493 spectrum in the UV, which is typical of unreddened Seyfert 1 galaxies. In particular, the continuum shape is nearly identical to that in the STIS spectrum of the unreddened Seyfert 1 galaxy NGC 4151 (Crenshaw et al. 2001). In addition, the emission lines (narrow plus broad) of Mrk 493 are essentially unreddened after correction for Galactic reddening; He II λ1640/λ4686 = 8.0 ± 1.9, which is consistent with the intrinsic ratio of 7 – 9 from

photoionization models of the NLR (Kraemer et al. 1994) and BLR (Rees, Netzer, & Ferland 1989)). The second assumption is based on the similarity of NLS1 galaxies in a number of properties, including their emission-line ratios (Osterbrock & Pogge 1985; Goodrich et al. 1989) and X-ray characteristics (Boller, Brandt, & Fink 1996; Leighly 1999). Obviously, this assumption needs to explored with a larger sample of simultaneous UV and optical observations of NLS1s, since there is likely to be intrinsic differences in the spectral energy distributions (SEDs) of these objects (the possible effects of these differences are discussed later in this section).

Most of the continuum and emission-line reddening of Akn 564 must be intrinsic, since the Galactic reddening is small. The maps of Galactic dust IR emission from Schlegel et al. (1998) give E(B−V) = 0.06, whereas a power-law plus Galactic extinction fit to the UV spectrum yields E(B−V) = 0.03 (S. Collier 2001, private communication) . We adopt the latter value (0.03), since correction of the observed spectrum for E(B−V) = 0.06 places the 2200 Å continuum region well above a smooth continuum fit (Figure 1). The Galactic reddening is small compared to the internal reddening (see below), so this choice has little effect on our results.

To determine the reddening curve for Akn 564, we follow the technique used by Crenshaw et al. (2001) in a study of the reddening and absorption in NGC 3227. The continuum fits in Figure 1 were each corrected for Galactic reddening, using E(B−V) = 0.03 and the standard Galactic curve (Savage & Mathis 1979). We can immediately determine the value of E(B−V) for the internal reddening: E(B−V) = 2.5 [log(X_B) − log(X_V)], where X is the ratio of the Mrk 493 continuum fit to that of Akn 564 as a function of wavelength, and is evaluated at the effective wavelengths of the B (4400 Å) and V (5500 Å) filters. From this relation, we find that E(B−V) = 0.14 mag for the internal reddening in Akn 564.

We can also determine the reddening curve at any wavelength, relative to V and as per convention normalized to E(B−V) (Savage & Mathis 1979):

$$\frac{E(\lambda - V)}{E(B - V)} \equiv \frac{A_\lambda - A_V}{A_B - A_V} = \frac{log(X_\lambda) - log(X_V)}{log(X_B) - log(X_V)}, \quad (1)$$

where A_B, A_V, and A_λ are the extinctions in magnitudes at B, V, and an arbitrary λ.

To determine the absolute extinction at any wavelength, we need to calibrate the above reddening curve:

$$\frac{A_\lambda}{E(B - V)} = \frac{E(\lambda - V)}{E(B - V)} + R_V, \quad (2)$$

by determining the offset $R_V \equiv A_V/E(B-V)$. We make use of the result that the stan-

dard Galactic, LMC, and SMC extinction laws have essentially the same values at $\lambda > 4500$ Å (Crenshaw et al. 2001, and references therein), and assume that this is the case for Akn 564. [15] Thus, R_V is the constant we need to add to $E(\lambda-V)/E(B-V)$ to match these laws at long wavelengths. This yields $R_V = 3.1$, which is also the standard Galactic value (Savage & Sembach 1979).

Figure 2 shows the extinction laws for the Galaxy, LMC, and SMC, along with the extinction law for Akn 564 determined in the fashion described above. The extinction curve for Akn 564 is unusual in that it diverges from the others at 4000 Å. At shorter wavelengths, the curve climbs steadily with no evidence for the sharp curvature seen in other laws in the far-UV; there is also no evidence for a 2200 Å bump, similar to the SMC curve (see §8). By comparison, the extinction curve for NGC 3227 also begins to diverge from the other curves at 3500 – 4000 Å, but rises even more sharply in the UV than the SMC curve (Crenshaw et al. 2001).

The principal uncertainty in the reddening curve of Akn 564 is likely the assumption that its intrinsic SED is identical to that of Mrk 493 (which, as noted earlier in this section, is essentially the same as that of NGC 4151 in an average state). Unfortunately, *HST* observations of other unreddened Seyfert 1 galaxies covering the full UV/optical range are not available to explore this issue. Therefore, we use the extreme variations of NGC 4151 itself, which was monitored extensively with *IUE*. Clavel et al. (1990) find that the ratio of UV to optical continuum $F_\lambda(1450)/F_\lambda(5000)$ varies by a factor of 3.1, with high ratios corresponding to high UV fluxes. However, Kaspi et al. (1996) find that a portion of this effect is due to a substantial galaxy contribution in the apertures used for optical observations; subtracting the stellar flux at 5000 Å leads to a ratio that varies by a factor of 2.1. Assuming this extreme variation for this ratio, the reddening value and uncertainity at 1450 Å is therefore $A_\lambda/E(B-V) = 11.1 \pm 2.5$. With this assumption, the reddening curve for Akn 564 could possibly be as shallow as the Galactic curve in the UV or somewhat steeper than the LMC curve, but not as steep as the curves for the SMC or NGC 3227. On the other hand, the extinction determined from the observed He II $\lambda1640/\lambda4686$ ratio is nearly identical to that derived for the continuum (§4.3) and the error in this ratio is only ∼30%, suggesting that the uncertainty in the reddening curve is much smaller than the conservative estimate quoted above.

[15] It would be preferable to match the continuum curves at $\lambda > 7000$ Å (Cardelli et al. 1989), but the FOS wavelength coverage for Akn 564 does not extend this far.

4. The Emission Lines

4.1. Measurements

We have measured the emission-line fluxes in the FOS spectrum of Akn 564 to determine the reddening from the He II lines and for a future investigation into the physical conditions in the emission-line regions and the spectral energy distribution (SED) of the ionizing continuum flux (P. Romano et al., in preparation). As is typical for Seyfert 1 galaxies, there are strong contributions to the spectrum from a high-density region responsible for lines such as Fe II (the classic BLR in normal Seyfert 1s) and a lower density region responsible for forbidden lines such as [O III] (the NLR). Since Akn 564 is a NLS1, these contributions are strongly blended together. Although the permitted lines tend to show broader wings than the forbidden lines, which is typical in these objects (Osterbrock & Pogge 1985; Goodrich 1989), they are not sufficiently broad to deconvolve the broad and narrow components, particularly at this spectral resolution. We therefore measured the total emission from each line.

We measured the emission line fluxes of most of the lines by direct integration of their fluxes over the continuum fit. For severe blends (e.g., Hα, [N II] λ6548, 6584), we used the [O III] λ5007 and Hβ profiles as templates for the forbidden and permitted lines, respectively, to deblend the emission features. For the UV lines affected by absorption, we used the emission-line fits from the STIS echelle spectra (see §5). We determined the line ratios relative to Hβ and corrected these ratios for reddening using the Akn 564 curve in Figure 2, with E(B−V) = 0.14 (±0.04), and the standard Galactic curve, with E(B−V) = 0.03 (our justification for using the Akn 564 continuum reddening curve is given in §4.3.) We determined errors in the dereddened ratios from the sum in quadrature of the errors from photon noise, different reasonable continuum placements, and reddening.

We show the observed and dereddened line ratios in Table 2. The C II λ1334 emission is undetectable in this object, whereas it is clearly seen in the UV spectra of most Seyfert galaxies (Crenshaw et al. 1999). There are no Galactic or intrinsic absorption features that could mask the C II emission. [O III] λ2321 and C II] λ2326 are not evident as well, but their absence could be explained by the presence of Galactic Fe II $\lambda\lambda$2374, 2382 absorption at the redshifted positions of these emission lines.

4.2. Spatial Extent of the NLR

To place a limit on the size of the NLR in Akn 564, we examined the two-dimensional STIS spectral images (there are no narrow-band *HST* images). We find that the spatial profiles of the continuum and strong emission lines (Lα, Mg II) along the slit are identical and indistinguishable from a point source (the spatial resolution is $0''.05$ – $0''.1$ FWHM in the UV). From the Lα spatial profile, we find that at least 85% of the emission-line flux must come from a region that is $\leq 0''.2$ (95 pc) from the nucleus (assuming circular symmetry). Thus, the NLR is compact (at least along this direction), which is often the case for Seyfert 1 galaxies (Schmitt & Kinney 1996).

4.3. Reddening of the Emission Lines

We can investigate the reddening of the emission lines in a manner independent of our continuum reddening analysis, since the ratios of the He II lines vary only slightly with temperature and density (Seaton 1978). The intrinsic He II $\lambda1640/\lambda4686$ ratio is $\sim$7 for the NLR (Kraemer et al. 1994) and $\sim$9 for the BLR (Rees et al. 1989). From this range and the observed ratio of 2.92 (corrected for Galactic reddening), the differential extinction is $A_\lambda(1640) - A_\lambda(4686) = 0.95$ – 1.22 mag, By comparison, the continuum extinction curve yields $A_\lambda(1640) - A_\lambda(4686) = 0.95$ mag. These values are in good agreement, although it is possible that the emission lines experience a slight amount of additional extinction (cf., Kraemer et al. 2000a). The similar extinctions for continuum and emission lines justifies our use of the continuum reddening curve in §4.1. The simplest explanation is a dust screen that lies outside of and covers both the continuum source and emission-line regions (including the NLR), similar to the situation for NGC 3227 (Crenshaw et al. 2001). One might expect that the intrinsic UV absorption lines could arise from gas associated with the dust; this possibility is explored in §7.

5. The Intrinsic UV Absorption

As noted in §2, the FOS spectra of Akn 564 show intrinsic absorption from Lα, N V, Si IV, and C IV; these lines are also seen in the low-dispersion STIS spectra (Collier et al. 2001). The STIS echelle spectra resolve these lines, as shown in Figure 3, which plots the absorption as a function of radial velocity (for the stronger member of the doublets) relative to the systemic redshift of z = 0.02467, determined from the H I 21-cm line (de Vaucouleurs, et al. 1991). We have also discovered the presence of intrinsic Si III $\lambda1206.5$ absorption at

the same approximate radial velocity as the Si IV absorption. However, there is no evidence for the presence of lower ionization lines, such as C II λ1334.5 or Si II λ1260.4. It is clear from Figure 3 that the Lα, N V, and C IV absorption lines are completely saturated, and there is no hope for separating individual kinematic components. Si IV and Si III appear not to be saturated, and common narrow kinematic components can be seen in these lines. Due to the noise and inherent difficulty in deblending these components, we treat the absorption as a single large kinematic component in our analysis. This treatment is appropriate if there are no large variations in the physical conditions as a function of radial velocity.

To measure the absorption lines, we fitted cubic splines to the continuum and emission lines, using the high signal-to-noise low-dispersion spectra as a guide. We then divided the echelle spectrum by the spline fit to normalize the absorption profiles. For the heavily saturated lines, we obtained a lower limit to C_{los}, the covering of the continuum plus emission by the absorber in the line of sight, from the residual flux (I_r) in the troughs: $C_{los} = 1.0 - I_r$. For Si IV, we determined the covering factor in the deepest portion of the lines with the doublet method of Hamann et al. (1997):

$$C_{los} = \frac{I_1^2 - 2I_1 + 1}{I_2 - 2I_1 + 1}, \tag{3}$$

where I_1 and I_2 are the residual fluxes in the cores of the weaker line (Si IVλ1402.8) and stronger line (Si IV λ1393.8) respectively.

The derived covering factors are given in Table 3. The values are very close to one, which indicates that all of the emission-line gas in this velocity range is occulted by the absorber. Since the narrow-line region (NLR) gas occupies this velocity range ($\pm$ 500 km s^{-1}, based on the optical [O III] lines), *the absorber must occult the NLR as well*. For example, based on the strengths of the forbidden [Ne V] lines (Table 2), we know that the NLR gas in this object is highly ionized, with an ionization parameter similar to that of the compact NLR in NGC 5548 (Kraemer et al. 1998). If we use the narrow C IV/[O III] ratio from NGC 5548 to estimate the narrow C IV flux in Akn 564, and assume the NLR is not covered, the C IV troughs reach an intensity of $\sim$0.5, instead of the observed value of zero seen in Figure 3.

The radial velocity centroids of the absorption lines are given in Table 3; these values are relative to the systemic redshift. The discrepant values can be attributed to the effects of saturation. The total column of gas is apparently smaller at more positive radial velocities, as indicated by the Si lines (assuming constant ionization parameter across the profiles). However, saturation will tend to fill in the red portions of the other absorption lines and shift the velocity centroids to less negative numbers. The best values for velocity centroid and full-width at half maximum (FWHM) weighted by column density are threfore obtained

from the unsaturated Si IV and Si III lines: $v_r = -194 \pm 5$ km s^{-1}, FWHM = 180 ± 20 km s^{-1}. On the other hand, the total velocity coverage of the absorber is best obtained from the heavily saturated Lα line: -420 to $+180$ km s^{-1}, relative to systemic. We note that the low-dispersion STIS and FOS spectra show no evidence for changes in radial velocity coverage (≥ 80 km s^{-1}) or equivalent width (≥ 0.2 Å) of the absorbers over the four-year interval between the observations.

Since the dust screen and UV absorber both cover the NLR, it is important to ascertain if they arise from the same region, and if they do, determine the physical conditions in this region. For this purpose, we have derived the ionic column densities (or limits) for the absorption. For the unsaturated lines, we determined the optical depth (τ) as a function of radial velocity (v_r) for a covering factor of one: $\tau = \ln (1/I_r)$. For the saturated lines, we assumed the minimum possible covering factor (0.97) to derive an absolute lower limit to the optical depth using the equation from Hamann et al. (1997):

$$\tau = ln \left(\frac{C_{los}}{I_r + C_{los} - 1} \right) \tag{4}$$

We then obtained the ionic column density (or lower limit) by integrating the optical depth across the profile:

$$N = \frac{m_e c}{\pi e^2 f \lambda} \int \tau(v_r) dv_r, \tag{5}$$

(Savage & Sembach 1991), where f is the oscillator strength and λ is the laboratory wavelength (Morton et al. 1988). We have also estimated upper limits to the two low ionization lines that we would expect to be strongest: C II λ1334.5 and Si II λ1260.4. The measured ionic column densites or limits are given in Table 3, along with model values discussed in the next section.

6. Photoionization Models of the Absorption

6.1. Model Parameters

Photoionization models for this study were generated using the code CLOUDY90 (Ferland et al. 1998). We have modeled the absorber as a matter-bounded slab of atomic gas, irradiated by the ionizing continuum radiation emitted by the central source. As per convention, the model is parameterized in terms of the ionization parameter, U, the ratio of the density of photons with energies ≥ 13.6 eV to the number density of hydrogen atoms (n_H) at the illuminated face of the slab. By matching the observed ionic column densities, we

can constrain the total hydrogen column density (N_H) and ionization parameter for the absorber. Of course, the value of N_H we obtain depends on our assumed elemental abundances (see below). The model is deemed successful when the predicted ionic columns match those observed to better than a factor of 2. As noted in §5, the strongest UV absorption lines (Lyα, C IV, and N V) are completely saturated, hence we only have lower limits to these ionic column densities. However, we can constrain the physical conditions in the absorber based on these limits, the columns of Si III and Si IV, and the upper limits for Si II and C II.

The X-ray continuum of Akn 564 is characterized by a strong excess below 1 keV, which has been variously modeled as thermal bremsstrahlung, a blackbody, a broad Gaussian, or as an absorption edge (Brandt et al. 1994; Turner, George, & Netzer 1999). There is evidence for a steep underlying power-law continuum, with a photon index $\Gamma \approx 2.5$ (Vaughan et al. 1999). As noted by Brandt et al. (1994), an extension of such a power-law greatly overpredicts the UV flux, hence the spectrum must flatten at energies below 0.1 keV. We based our derived model SED on the observed fluxes at 1150 Å and 0.5 keV, assuming that the continuum consists of power laws of the form $L_\nu \propto \nu^{-\alpha}$, where $\alpha = 1.0$ at $h\nu <$ 13.6 eV, $\alpha = 1.07$ between 13.6 eV and 0.5 keV, and $\alpha = 1.6$ at $h\nu > 0.5$ keV (consistent with the 0.7 – 3 keV fluxes measured by Turner et al. [2001a]). To account for the soft X-ray excess, we also included a blackbody of temperature $kT = 0.157$ keV, similar to that derived for the luminous NLS1 Ton S180 (Turner et al. 2001b). The blackbody was scaled to contribute 1/3 of the flux at 0.5 keV, as suggested by Turner et al. (2001a), and is the simplest representation of the SED, given the lack of evidence for a turn-over (Turner et al. 2001a). Based on this SED, we estimate the central source luminosity in ionizing photons is $\approx 2.0 \times 10^{54}$ s^{-1}. Note that this is ~ 13 times the luminosity of the Seyfert 1 galaxy NGC 3227 (Kraemer et al. 2000b), and most likely a conservative lower limit, since we have assumed that the continuum does not peak below 0.1 keV. Figure 4 shows the incident and transmitted continua for the models (see §6.2).

We have also assumed roughly solar abundances (cf. Grevesse & Anders 1989) by number relative to H, as follows: He = 0.1, C = 3.4 x 10^{-4}, N = 1.2 x 10^{-4}, O = 6.8 x 10^{-4}, Ne = 1.1 x 10^{-4}, Mg = 3.3 x 10^{-5}, Al = 2.96 x 10^{-6}, Si = 3.1 x 10^{-5}, P = 3.73 x 10^{-7}, S = 1.5 x 10^{-5}, Fe = 4 x 10^{-5}, and Ni = 1.78 x 10^{-6}. Given the evidence for a large column of dusty gas and the absence of C II in absorption, we have used a standard depletion of 85% of the carbon onto grains (Draine & Lee 1984). However, the presence of Si III in absorption argues against the presence of silicate grains, and we have therefore assumed no depletions of other elements. [16]

[16]The presence of carbon grains without silicate grains is an empirical assumption that provides a good

6.2. Model Results

We modeled the UV absorber as a single-zone and arrived at the following best-fit parameters: U = 0.033 and N_H = 1.62 x 10^{21} cm^{-2}. The predicted ionic columns are listed in Table 3 and, generally, provide a good fit to the observed column densities. The predictions for Lyα, C IV, and N V exceed the lower limits, while those for C II and Si II are consistent with their upper limits. The predicted column for Si IV is close to the observed value and, although the predicted Si III column is somewhat high, it is within a factor of 2 of that observed. In Table 4, we list predicted column densities for the ions C III, N III, and O VI, which can produce absorption lines observable in the *FUSE* bandpass (910 – 1185 Å), and O VII and O VIII, from which strong bound-free edges and absorption lines associated with "warm" absorbers arise (Reynolds 1997; George et al. 1998). Based on the most recent *ASCA* spectra (Turner et al. 2001a), we determined upper limits for the bound-free optical depths and column densities of O VII ($\tau_{OVII} \leq 0.054$, $N_{OVII} \leq 2.2$ x 10^{17} cm^{-2}) and O VIII ($\tau_{OVIII} \leq 0.001$, $N_{OVIII} \leq 1.1$ x 10^{16} cm^{-2}), which are consistent with our model predictions.

7. The Connection Between UV Absorption and Reddening

The total hydrogen column in our model would yield a reddening value of E(B−V) = 0.31 for a Galactic dust-to-gas ratio, from the relation given by Shull & Van Steenberg (1985). Our derived internal reddening for this object is E(B−V) = 0.14, which is consistent with the lower than Galactic dust-to-gas ratio in our model, due to the absence of silicate grains. In any case, the UV absorber has enough column to produce the observed reddening. Given that the UV absorber covers the NLR in Akn 564, the dusty gas must lie further than 95 pc from the active nucleus (see §4.2) and have a density of $n_H \leq 10^3$ cm^{-3} based on our model parameters.

There are two additional considerations that must be addressed. First, although the models show that the UV absorption is consistent with carbon depletion, the spectrum of Akn 564 shows no evidence for a 2200 Å extinction feature. However, this feature is typically

---

match to the observed ionic column densities (§6.2). To our knowledge, this situation has not been seen in other types of objects, and may reflect the unusual environment around a Seyfert nucleus. Interestingly, the C II λ1334.5 emission line is not detected and the C IV λ1550 and C III] λ1909 emission lines appear to be relatively weak in Akn 564 compared to lines such as N V λ1240, N III] λ1750 and Si III] λ1890 (Table 2). Although this could result from a combination of high densities (Kuraszkiewicz et al. 2000) and unusual abundance ratios (Wills et al. 1999; Mathur 2000), another explanation is that the carbon has been removed from gas phase by depletion onto dust grains.

absent in reddened AGN (Pittman, Clayton, & Gordon 1999), and, in any event, its origin is not well understood. Second, since emission-lines will arise in the absorber, its covering factor is constrained by the observed emission-line fluxes. For example, the absorber we have modeled at a radial distance of 95 pc would require a global covering factor of 0.05 to account for all of the observed [Ne V] λ3426 and 80% of [O III] λ5007. Since there may be significant [O III] λ5007 emission from the gas in which low ionization lines such as [N II] λ6584 and [O II] λ3227 form (see Kraemer et al. 2000a), the covering factor of the absorber may be somewhat less than this value.

To summarize, the absorber is of sufficiently high ionization state to produce saturated N V and C IV absorption lines. We predict O VII and O VIII column densities much lower than that associated with the "warm" absorbers detected in *ASCA* spectra of Seyfert 1 galaxies (Reynolds 1997; George et al 1998). Hence, we arrive at the same conclusion as that for the Seyfert 1 galaxy NGC 3227 (Kraemer et al. 2000b; Crenshaw et al. 2001): the dust is embedded in a "lukewarm absorber" which lies outside of the NLR.

8. Discussion

Our motivations for this study were to investigate the intrinsic UV absorption revealed in the FOS archive spectra of Akn 564, and observed at high resolution with STIS during the recent monitoring campaign, and to evaluate the reddening of the UV continuum fluxes for a study of the intrinsic SED (P. Romano et al., in preparation). In doing so, we have discovered that the intrinsic absorption and reddening are linked in this object, in that the absorbing gas has a sufficient column (N_H = 1.6 x 10^{21} cm^{-2}) and distance from the continuum source (D > 95 pc) to contain the dust that reddens the continuum source, BLR, and compact NLR. The properties of the absorbing gas in Akn 564 are very similar to those in the dusty lukewarm absorber in NGC 3227 (N_H = 2.0 x 10^{21} cm^{-2}, D > 92 pc; Crenshaw et al. 2001), suggesting a common origin. One interesting difference, however, is the derived reddening curve; in NGC 3227, it is much steeper in the UV, suggesting a preponderence of small dust grains (Crenshaw et al. 2001). Simultaneous UV/optical spectra of additional reddened Seyfert galaxies, covering a broad wavelength range (e.g., 1150 – 10,000 Å) at high spatial resolution ($\sim$0$''$.1, to minimize contamination by the host galaxy) would be helpful in exploring the range of reddening curves in Seyferts.

The ionization state of the gas is relatively high in both NGC 3227 (U = 0.13) and Akn 564 (U = 0.032), but not high enough (given the N_H columns) to produce observable O VII and O VIII edges detectable by *ASCA* (although possibly detectable through absorption lines in *Chandra* spectra). Thus, these absorbers do not qualify as "dusty warm

absorbers", which have been claimed in several AGN, including NGC 3227 (Komossa & Fink 1997). As noted in Kraemer et al. (2000b) and Crenshaw et al. (2001), the dusty lukewarm absorber provides a more natural explanation, since it can be placed at large distances (> 100 pc) from the nucleus and account for not only the reddening of the continuum source and BLR, but the observed reddening of the NLR as well. As in the case of NGC 3227 and Akn 564, the dusty lukewarm absorber can be identified in reddened sources through the detection of strong UV absorption lines near the systemic redshift.

Dusty lukewarm absorbers likely originate from a different location than the majority of known intrinsic absorption systems in Seyfert 1 galaxies. The latter tend to be variable and, in many cases, exhibit high outflow velocities (up to 2100 km s^{-1}, Crenshaw et al. 1999), indicating an origin close to the nucleus. On the other hand, the dusty lukewarm absorbers in the two objects we have studied are located outside of the majority of the NLR emission. Interestingly, the galactic disks of both Seyferts are inclined to our line of sight ($i = 63^{o}$ for NGC 3227, $i = 59^{o}$ for Akn 564; De Zotti & Gaskell 1985), yielding a line of sight with a larger optical depth that intercepts more of the host galaxy's disk compared to face-on ($i \approx 0$) Seyfert galaxies. There is ample morphological and kinematic evidence that the extended narrow-line region (ENLR) in a Seyfert galaxy is ionized gas in the galactic disk (cf., Unger et al. 1987). Thus, it is likely that the dusty lukewarm absorber is a highly ionized component in the ENLR that we see when looking through the host galaxy's disk.

This work was supported by NASA through grant number HST-GO-08265.02-A from the Space Telescope Science Institute, which is operated by the Association of Universities for Research in Astronomy, Inc., under NASA contract NAS5-26555. DMC and SBK acknowledge support from NASA guaranteed time observer funding to the STIS Science Team under NASA grant NAG5-4103. WNB acknowledges support from NASA LTSA grant NAG5-8107. This research has made use of the NASA/IPAC Extragalactic Database (NED) which is operated by the Jet Propulsion Laboratory, California Institute of Technology, under contract with the National Aeronautics and Space Administration.

REFERENCES

Boller, T., Brandt, W.N., & Fink, H. 1996, A&A, 305, 53

Boroson, T.A., & Green, R.F. 1992, ApJS, 80, 109

Brandt, W.M., Fabian, A.C., Nandra, K., Reynolds, C.S., & Brinkmann, W. 1994, MNRAS, 271, 958

Brandt, W.M., Fabian, A.C., & Pounds, K.A. 1996, MNRAS, 278, 326

Cardelli, J.A., Clayton, G.C., & Mathis, J.S. 1989, ApJ, 345, 245

Clavel, J., et al. 1990, MNRAS, 246, 668

Collier, S., et al. 2001, ApJ, in press

Crenshaw, D.M., Kraemer, S.B., Boggess, A., Maran, S.P., Mushotzky, R.F., & Wu, C.-C. 1999, ApJ, 516, 750

Crenshaw, D.M., Kraemer, S.B., Bruhweiler, F.C., & Ruiz, J.R. 2001, ApJ, 555, 633

de Vaucouleurs G., de Vaucouleurs A., Corwin H. G., Buta R. J., Paturel, G., & Fouque P. 1991, Third Reference Catalogue of Bright Galaxies Springer-Verlag, New York

De Zotti, G., & Gaskell, C.M. 1985, A&A, 147, 1

Draine, B.T., & Lee, H.M. 1984, ApJ, 285, 89

Ferland, G.J. et al. 1998, PASP, 110, 761

George, I.M., Turner, T.J., Netzer, H., Nandra, K., Mushotzky, R.F., & Yaqoob, T. 1998a, ApJS, 114, 73

Goodrich, R.W. 1989, ApJ, 342, 224

Grevesse, N. & Anders, E. 1989, in Cosmic Abundances of Matter, ed. C.J. Waddington (New York: AIP),1

Hamann, F., Barlow, T.A., Junkkarinen, V., & Burbidge, E. M. 1997, ApJ, 478, 78

Hutchings, J.B. 1982, ApJ, 255, 70

Kaspi, S., et al. 1996, ApJ, 470, 336

Kuraszkiewicz, J., Wilkes, B.J., Czerny, B., & Mathur, S. 2000, ApJ, 542, 692

Komossa, S., & Fink, H. 1997, A&A, 327, 483

Koornneef, J., & Code, A.D., 1981, ApJ, 247, 860

Kraemer, S.B., Crenshaw, D.M., Peterson, B.M., & Filippenko, A.V. 1998, ApJ, 499, 719

Kraemer, S.B., Crenshaw, D.M., Hutchings, J.B., Gull, T.R., Kaiser, M.E., Nelson, C.H., & Weistrop, D. 2000a, ApJ, 531, 278

Kraemer, S.B., George, I.M., Turner, T.J., & Crenshaw, D.M. 2000b, ApJ, 535, 53

Kraemer, S.B., Wu, C.-C., Crenshaw, D.M., & Harrington, J.P. 1994, ApJ, 435, 171

Leighly, K.M. 1999, ApJS, 125, 297

Lindler, D. 1998, CALSTIS Reference Guide (CALSTIS Version 5.1)

Mathur, S. 2000, MNRAS, 314, L17

Morton, D.C., York, D.G., & Jenkins, E.B. 1988, ApJS, 68, 449

Osterbrock, D.E., & Pogge, R.W. 1985, ApJ, 297, 166

Pittman, K.M., Clayton, G.C., & Gordon, K.D. 1999, PASP, 112, 537

Pounds, K.A., et al. 2001, ApJ, in press

Rees, M.J., Netzer, H., & Ferland, G.J. 1989, ApJ, 347, 640

Reynolds, C.S. 1997, MNRAS, 286, 513

Savage, B.D., & Mathis, J.S. 1979, ARAA, 17, 73

Savage, B.D., & Sembach, K.R. 1991, ApJ, 379, 245

Schlegel, D.J., Finkbeiner, D.P., & Davis, M. 1998, ApJ, 500, 525

Schmitt, H.R., & Kinney, A.L. 1996, ApJ, 463, 498

Seaton, M.J. 1978, MNRAS, 185, 5P

Shemmer, O., et al. 2001, ApJ, in press

Shull, J.M., & Van Steenberg, M.E. 1985, ApJ, 294, 599

Turner, T.J., George, I.M., & Netzer, H. 1999, ApJ, 526, 52

Turner, T.J., et al. 2001a, ApJ, in press

Turner, T.J., George, I.M., Yaqoob, T., Kriss, G., Crenshaw, D.M., Kraemer, S., Zheng, W., Wang, J., & Nandra, K. 2001a, ApJ 548, L13

Unger, S.W., et al. 1987, MNRAS, 228, 671

Vaughan, S., Reeves, J., Warwick, R., & Edelson, R. 1999, MNRAS, 309, 113

Walter, R., & Fink, H.H. 1993, A&A, 274, 105

Wills, B.J., Laor, A., Brotherton, M.S., Wills, D., Wilkes, B.J., Ferland, G.J., & Shang, Z. 1999, ApJ, 515, L53

Wills,B.J., Netzer, H., & Wills, D. 1985, ApJ, 288, 94

AAS LaTeX macros v5.0.

Fig. 1.— FOS UV/optical spectra of two narrow-line Seyfert 1 galaxies. The spectrum of Mrk 493 has been scaled by a factor of 3.0 to match the continuum flux of Akn 564 at 5500 Å, and has been offset by 3.0 x 10^{-14} ergs s^{-1} cm^{-2} $Å^{-1}$. The smooth curves are continuum fits.

Fig. 2.— Reddening curve for Akn 564 as a function of wavelength (solid line). Reddening curves for the Galaxy (the standard curve of Savage & Mathis 1979), LMC (Koornneef & Code 1981), and SMC (Hutchings 1982) are given for comparison.

Fig. 3.— Portions of the STIS echelle spectra of Akn 564, showing the intrinsic UV absorption lines detected. Fluxes are plotted as a function of radial velocity (of the strongest line for the N V, C IV, and Si IV doublets), relative to a systemic redshift of z = 0.02467. The weaker members of the doublets at longer wavelengths are also visible.

Fig. 4.— Incident (solid line) and transmitted (dashed line) continua for the model described in the text.

Table 1. *HST* Spectra of Akn 564

Instr.	Grating	Aperture	Coverage (Å)	R.P.[a] ($\lambda/\Delta\lambda$)	Exposure (sec)	Date (UT)
FOS	G130H	0″.86 diameter	1150 – 1605	1300	3550	1996 May 23
FOS	G190H	0″.86 diameter	1572 – 2312	1300	1500	1996 May 23
FOS	G270H	0″.86 diameter	2222 – 3277	1300	1200	1996 May 23
FOS	G400H	0″.86 diameter	3235 – 4781	1300	910	1996 May 23
FOS	G500H	0″.86 diameter	4569 – 6817	1300	590	1996 May 23
STIS	G140L	52″ x 0″.5	1150 – 1714	1200	55,434[b]	2000 May 9 - July 8
STIS	G230L	52″ x 0″.5	1600 – 3145	800	24,216[b]	2000 May 9 - July 8
STIS	E140M	0″.2 x 0″.2	1150 – 1710	46,000	10,310	2000 May 29

[a]Resolving Power ($\lambda/\Delta\lambda$) at the central wavelength of each spectrum.

[b]Total exposure time for spectra averaged over 46 visits.

Table 2. Akn 564 Emission-Line Ratios (relative to Hβ[a])

Line	Observed Ratio	Reddening Corrected[b]
Lα λ1216	4.21 ±0.47	15.77 ±4.80
N V λ1240	1.18 ±0.16	4.34 ±1.32
O I λ1302	0.27 ±0.06	0.95 ±0.29
O IV] + Si IV λ1400	0.35 ±0.07	1.16 ±0.34
N IV] λ1486	0.25 ±0.05	0.78 ±0.22
C IV λ1550	1.13 ±0.16	3.39 ±0.91
He II λ1640	0.55 ±0.08	1.59 ±0.41
O III] λ1663	0.21 ±0.03	0.60 ±0.15
N III] λ1750	0.23 ±0.04	0.63 ±0.16
Si III] λ1890	0.10 ±0.02	0.25 ±0.06
C III] λ1909	0.40 ±0.05	1.07 ±0.24
[Ne IV] λ2423	0.09 ±0.02	0.19 ±0.04
[Fe XI] λ2649	0.04 ±0.01	0.07 ±0.02
Mg II λ2800	0.58 ±0.08	1.04 ±0.16
O III λ3133	0.18 ±0.06	0.29 ±0.06
[Ne V] λ3346	0.06 ±0.01	0.08 ±0.01
[Ne V] λ3424	0.16 ±0.02	0.23 ±0.03
[Fe VII] λ3588	0.02 ±0.01	0.03 ±0.01
[O II] λ3727	0.12 ±0.02	0.15 ±0.02
[Fe VII] λ3760	0.05 ±0.01	0.06 ±0.01
[Ne III] λ3869	0.11 ±0.01	0.13 ±0.02
H 8 + He I λ3889	0.05 ±0.01	0.06 ±0.01
[Ne III] + Hϵ λ3967	0.11 ±0.02	0.13 ±0.02
[S II] λ4072	0.03 ±0.01	0.03 ±0.01
Hδ λ4100	0.17 ±0.03	0.20 ±0.03
Hγ λ4340	0.32 ±0.05	0.35 ±0.06
[O III] λ4363	0.06 ±0.02	0.06 ±0.02
He II λ4686	0.21 ±0.05	0.22 ±0.05
Hβ λ4861	1.00	1.00
[O III] λ4959	0.30 ±0.04	0.30 ±0.04

Table 2—Continued

Line	Observed Ratio	Reddening Corrected[b]
[O III] λ5007	0.98 ±0.12	0.96 ±0.12
[Fe VII] λ5721	0.04 ±0.01	0.03 ±0.01
He I λ5876	0.08 ±0.02	0.07 ±0.02
[Fe VII] λ6087	0.05 ±0.02	0.04 ±0.02
[O I] λ6300	0.07 ±0.01	0.06 ±0.01
[Fe X] λ6374 + [O I] λ6364	0.14 ±0.03	0.12 ±0.03
Hα λ6563	4.57 ±0.50	3.78 ±0.53
[N II] λ6584	0.15 ±0.05	0.12 ±0.05

[a]Reddening-Corrected Flux (Hβ) = 3.13 (± 0.34) x 10^{-13} ergs cm^{-2} s^{-1}.

[b]Lines corrected using $E_{B-V} = 0.14 \pm 0.04$ and Akn 564 reddening curve from Figure 2 plus $E_{B-V} = 0.03$ and Galactic curve.

Table 3. Intrinsic Absorption – Measurements and Models

Ion	C_{los}	v_r[a] (km s^{-1})	N (Observed) (cm^{-2})	N (Model[b]) (cm^{-2})
H I	1.00 ±0.03	−106	$> 1.4 \times 10^{15}$	5.0×10^{17}
N V	1.00 ±0.03	−152	$> 3.1 \times 10^{15}$	4.7×10^{16}
C IV	1.00 ±0.02	−130	$> 2.5 \times 10^{15}$	1.4×10^{16}
Si IV	0.99 ±0.01	−197	1.6×10^{14}	1.5×10^{14}
Si III	——	−190	2.6×10^{13}	4.8×10^{13}
C II	——	——	$< 5.4 \times 10^{13}$	5.5×10^{13}
Si II	——	——	$< 7.4 \times 10^{12}$	1.7×10^{12}

[a]velocity centroid relative to the systemic redshift of 0.02467

[b]U = 0.032, $N_H = 1.62 \times 10^{21}$ cm^{-2}

Table 4. Additional Predicted Ionic Column Densities

Ion	(cm^{-2})
C III	5.2×10^{15}
N III	1.5×10^{16}
O VI	2.4×10^{17}
O VII	1.5×10^{17}
O VIII	5.3×10^{15}

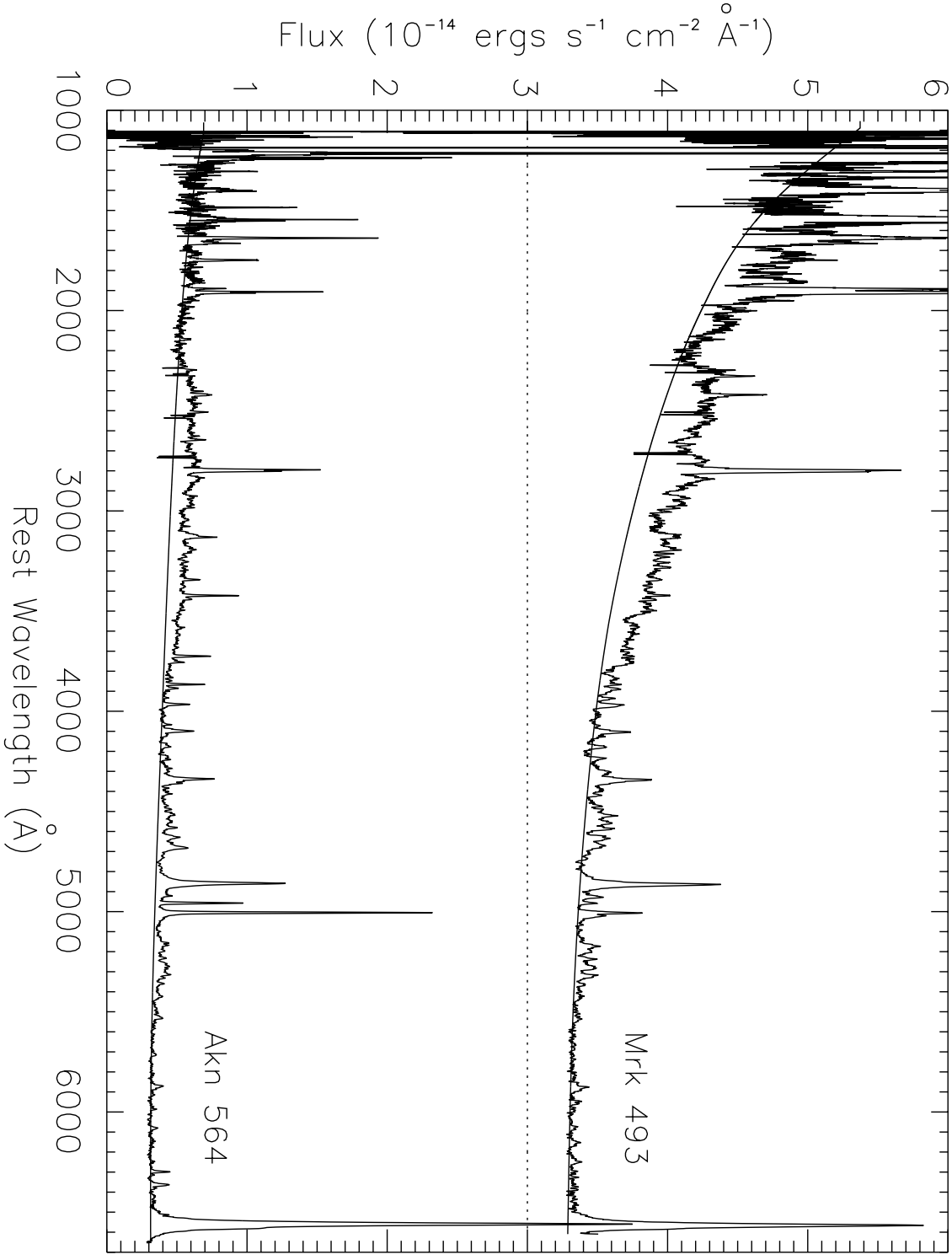
Flux (10^{-14} ergs s^{-1} cm^{-2} Å^{-1})
0
1
2
3
4
5
6
1000
2000
3000
4000
5000
6000
Rest Wavelength (Å)
Akn 564
Mrk 493

Fig. 1.

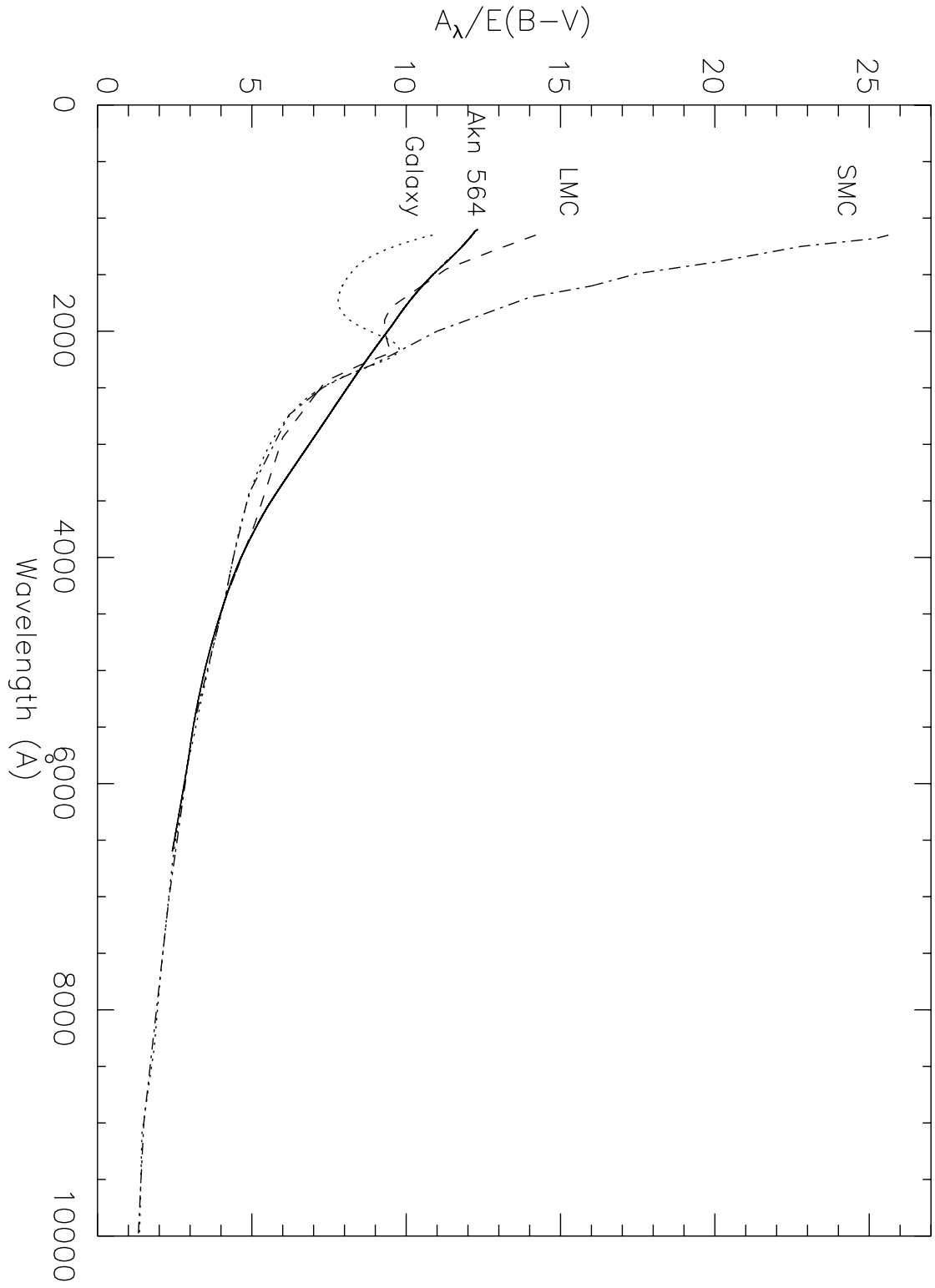
$A_\lambda/E(B-V)$
0
5
10
15
20
25
Galaxy
Akn 564
LMC
SMC
0
2000
4000
6000
8000
10000
Wavelength (A)

Fig. 2.

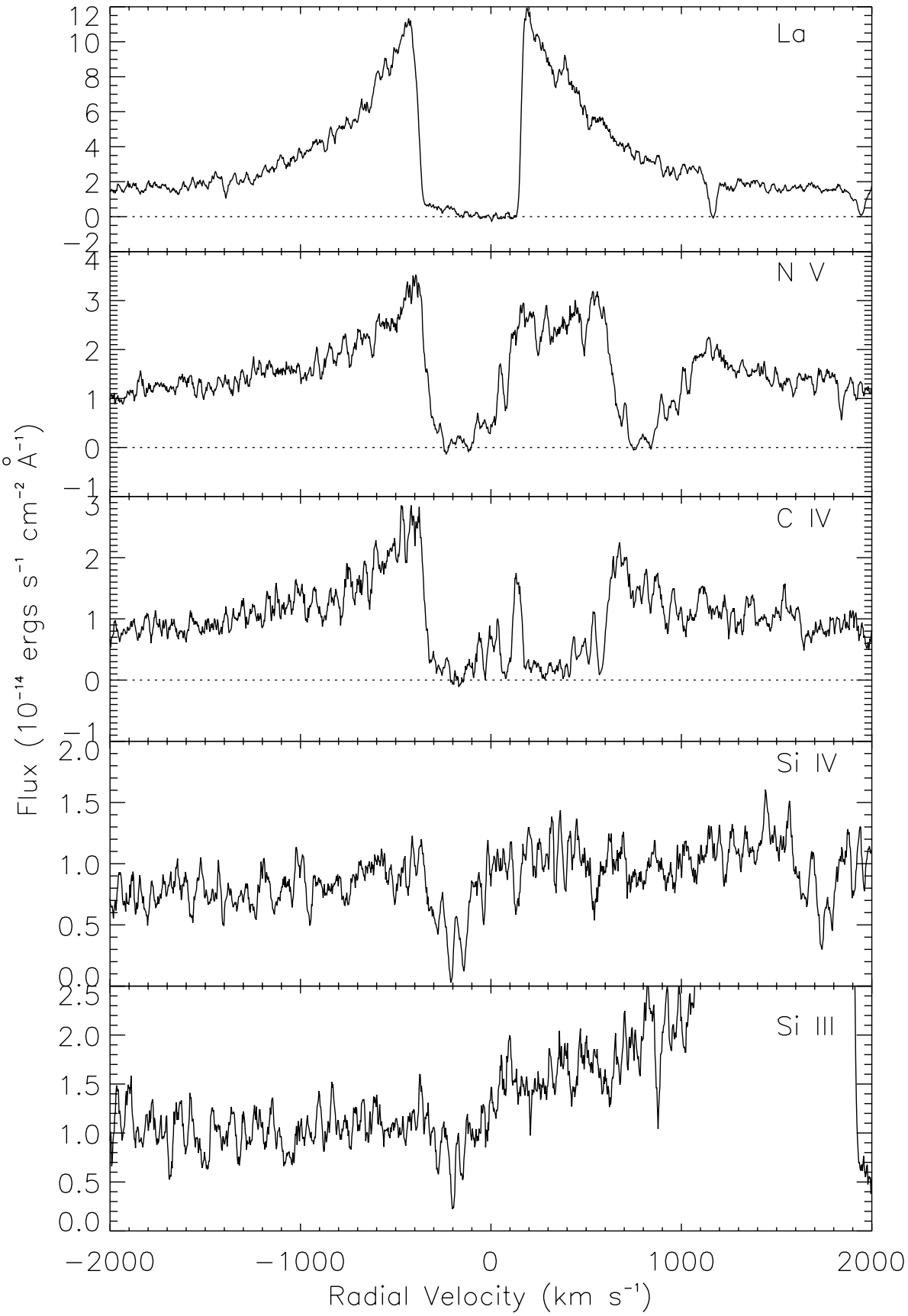
La
N V
C IV
Si IV
Si III
Flux (10^{-14} ergs s^{-1} cm^{-2} Å^{-1})
Radial Velocity (km s^{-1})
−2000
−1000
0
1000
2000

Fig. 3.

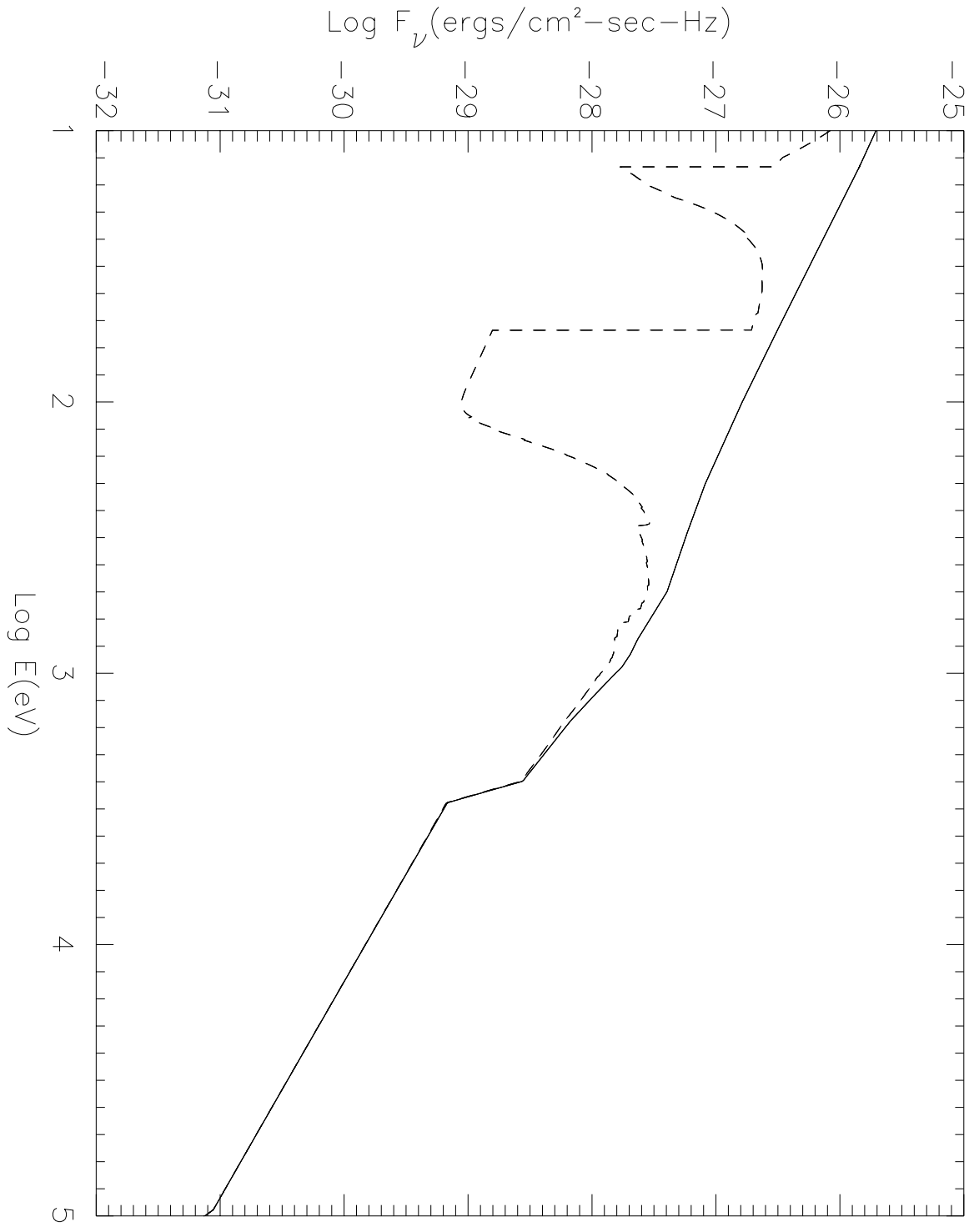

Fig. 4.